International Forum on Aeroelasticity and Structural Dynamics
IFASD 2024
17-21 June 2024, The Hague, The Netherlands

DESIGN AND EXPERIMENTAL CHARACTERIZATION OF A GUST-GENERATOR CONCEPT WITH ROTATING-SLOTTED CYLINDERS IN THE LOW-SPEED WIND TUNNEL DNW-NWB

Thomas G. Schmidt[1], Johannes Dillinger[1], Markus Ritter[1], Anna Altkuckatz[1], Charlotte Hanke[1], Marc Braune[1], Wolf R. Krüger[1], Holger Mai[1]

[1]German Aerospace Center (DLR), Institute of Aeroelasticity
Bunsenstraße 10, 37073 Göttingen, Germany
tg.schmidt@dlr.de
holger.mai@dlr.de

Keywords: Gust-generator design, structural modeling, gust-flow aerodynamics, experimental aeroelasticity

Abstract: The present study focuses on the design of a gust generator based on stationary airfoils coupled with downstream rotating, slotted cylinders, specifically configured for the low-speed wind tunnel DNW-NWB. Owing to the technical requirements imposed by the test facility and the desired gust characteristics, this particular gust-generator concept is chosen. Numerical computations for both wake-flow characteristics and structural properties are performed, so as to explore various design parameters. In a subsequent step, an experimental test campaign is conducted, in which the gust generator's wake flow is characterized using an unsteady fast-response 5-hole probe. The results reveal that highly periodic gust flows are induced by the gust generator, with gust amplitudes that are sufficiently large for investigating the gust response of flexible aircraft structures, e.g., wings. Besides, the gust frequency is directly proportional to the cylinders rotational speed, whether a continuous or discrete gust is generated. Future work is dedicated towards further enhancing the present gust generator, including - but not limited to - the motor's controls that drive the rotating cylinders.

1 INTRODUCTION

The global climate change is an omnipresent challenge faced by all industries that requires novel solutions to reduce emissions. To address this challenge, the European Union developed a long-term strategy to achieve carbon neutrality by 2050, which calls to action all (economic) sectors - among which the aerospace industry. Its particular goal is to achieve a greener, commercial air travel, which calls upon manufacturers to develop novel aircraft concepts that would allow for a more efficient in-flight performance. More specifically, this is achieved through lower drag and/or structural mass, so as to reduce an aircraft's fuel consumption and, in turn, its carbon footprint. Recently, one common approach is to increase the aircraft's wingspan (i.e., reach a higher aspect ratio), which would incur lower induced drag, albeit at the cost of higher wing mass - an drawback necessary due to the exacerbated structural loads. It is therefore pivotal to develop novel techniques that can alleviate these loads, particularly those occurring during extreme events, e.g., in-flight maneuvers and/or wind gusts. This being said, the latter's impact onto aircraft wings, especially their aeroelastic behavior, gust load tests were commonly explored using complex numerical means with fluid-structure coupling (e.g., [1–5]). While these

provided key insights into the wing's aeroelastic response under inflow gusts, this interaction is particularly challenging to model numerically, due to its unsteady and dynamic nature. Consequently, experimental research efforts were sought after that focus on a wing's aeroelastic response with respect to gusts, at the very least so that numerical researchers can validate their computations. Notably, to obtain a gust flow in wind tunnel experiments, a specific device is needed - a so-called gust generator.

At this stage, it is worth noting that such gust generators come in various shapes and sizes, their design being driven by several factors, including - but not limited to - the test facility's dimensions, experimental requirements regarding the gust flow, manufacturing cost, design complexity, and/or maintenance. The most common concept revolves around oscillating or pitching airfoil profiles/vanes [4–10] that would deflect the incoming flow, thereby generating a periodic wake pattern. While these are found to achieve large gust angles (i.e., amplitudes), they may be limited in terms of the feasible size and, thus, may be challenging to employ in large tunnel test sections. More precisely, as the tunnel's test section expands, the pitching airfoils would become large - both in terms of span and chord - thus not only requiring higher structural rigidity due to the increased loads, but also needing a more powerful actuator owing to the high torque. Upon this, other gust-generator concepts were developed, which - among others - include those based on oscillating wall fences [11], a vortex-generator array [12], a movable plate [13], and fixed airfoils with rotating slotted cylinders (RSC) at their trailing edge [14–16]. In particular, this latter concept was found to reduce the system's mechanical complexity, whilst allowing for a more controllable and reliable gust-flow generation [16]. These characteristics are deemed critical for the design and application of such a gust generator to be installed in large-scale test sections, e.g., that of the low-speed wind tunnel located in Braunschweig, namely the DNW-NWB - which, up to now, did not feature such a device.

To fill this gap, the present work describes the design, manufacturing, and subsequent experimental characterization of an airfoil-RSC-type gust generator that is specifically configured for the large test section of the DNW-NWB wind tunnel. Besides, to capture various gust conditions, this novel gust-generator device is capable of inducing continuous as well as discrete gust events of variable frequencies. This test rig is developed as part of the project *oLAF* (optimized load-adaptive aircraft) by the German Aerospace Center (DLR), whose goal is to characterize the gust response of a flexible wing model and evaluate the performance of gust-load alleviation (GLA) control techniques during an extensive experimental test campaign. At this stage, the reader is referred to the related works coming from the *oLAF* project, which respectively detail the overall project objective [17], the design of the test model (i.e., an actively-controlled, flexible aircraft wing configuration [18]), and the controller design and implementation for gust-load alleviation [19]. The present paper is organized as follows: Section 2 describes the conceptual design of the airfoil-RSC gust generator, before its characteristics are numerically explored in terms of its wake-flow topology (Section 3) and its structural behavior (Section 4) and subsequently validated during an experimental campaign (Section 5). Finally, conclusions and perspectives are provided in Section 6.

2 CONCEPTUAL DESIGN

Upon the portrayed literature, various gust-generator designs were explored that could effectively produce inflow gusts. Nonetheless, the gust-flow characteristics of each generator were specifically targeted to replicate certain real-life conditions, among which to study the gust response of aircraft wings [4, 9, 11], wind turbine blades [20], or micro aerial vehicles [21]). In the present case, the aeroelastic response of aircraft wings under gust loading is sought after, for which novel gust-load alleviation techniques (e.g., controllers as done in the oLAF project -

see [4]) are explored. To this end, the present device shall be able to induce a continuous gust flow in its wake, which is of variable frequency $f_g = 3 - 12\,\mathrm{Hz}$ and sufficiently pronounced amplitude - or gust angle. Besides, the certification requirements for gust flows imposed by the European Union Aviation Safety Agency (EASA - CS25, [22]) stipulate that large aircraft need to withstand discrete gusts of *1-cos* shape.

Aside from the technical specifications considered, the wind tunnel facility (i.e., the DNW-NWB) also comes with its own challenges, these referring primarily to its height. Indeed, to span the full test section, the present gust generator must be structurally stiff enough to withstand the aerodynamic loading exerted by the inflow wind, as well as unsteady forces associated with the gust-flow generation mechanism, which would ultimately cause the gust generator to bend. Besides, the required size and weight of the generator would necessitate actuators (i.e., motors) that can produce high torques coupled with high rotational speeds.

Following the described requirements and limitations, a gust generator based on stationary airfoils with rotating, slotted cylinders downstream of their trailing edges is opted for (cf. the principle sketch in Fig. 1), instead of more conventional designs using pitching airfoil vanes. More specifically, this airfoil-RSC concept allows for highly flexible gust flow characteristics, whether this concerns continuous or discrete gusts, whilst being rather simple in terms of its overall mechanical design and installation. The slotted cylinder design induces a gust frequency (ω_g) that is twice that of the rotational speed (ω). Notably, the flexibility of this particular concept stems from the various design parameters that would affect the gust generation and, thus, are explored through preliminary experimental and numerical campaigns. Several of these parameters are outlined in Fig. 1, among which the cylinder's rotational speed and orientation (ω), the gap between airfoil and RSC (e), the spacing between two adjacent airfoils (s), and the distance between the gust generator and the observer point, or position of the test model, in its wake (d_i). It is worth noting that the gust-generator concept developed here comprises four airfoil-RSC units, of which however only two have been realized at this stage.

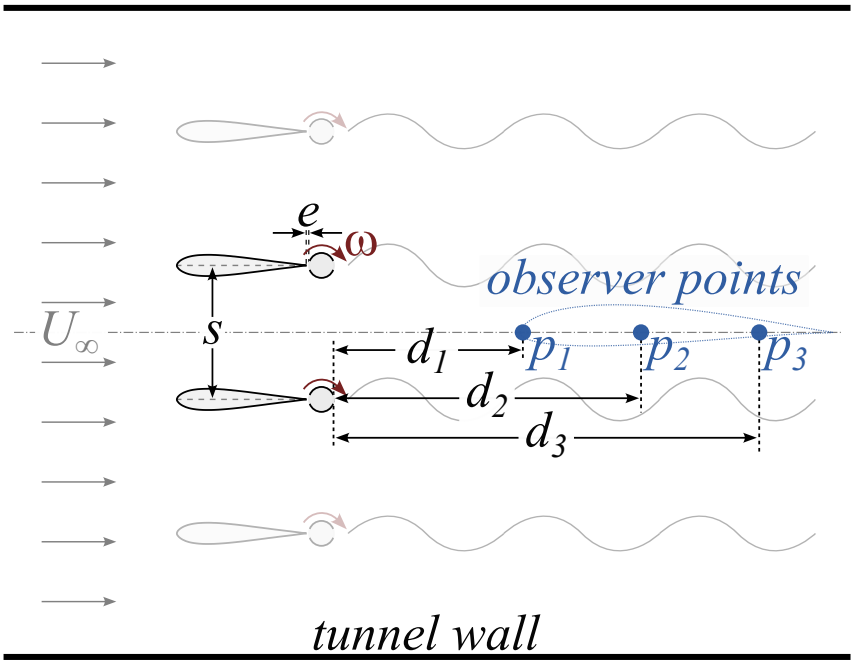

Figure 1: Schematic of the gust-generator setup in the tunnel vein, illustrating various design parameters, among which three observer points (p_1 - p_3), at which wake measurements are obtained.

3 NUMERICAL CHARACTERIZATION

In this section the aerodynamic characteristics of the airfoil-RSC gust generator are numerically explored, with a special emphasis on the influence of the design parameters onto the aerodynamic performance and wake-flow topology. This is done using numerical means, namely Computational Fluid Dynamics (CFD) simulations.

3.1 Computational Methodology & Setup

To obtain the gust generator's wake flow characteristics, two-dimensional (2D) URANS CFD simulations are employed based on DLR's in-house CFD solver *TAU*, with Menter SST $k-\omega$ and γ-CAS models for flow turbulence and transition, respectively. The computational domain and the CFD grid of these preliminary studies are shown in Fig. 2, including two fixed airfoils/wings based on the NACA 63010 profile, each of which is followed by a rotating slotted cylinder. These airfoils as well as the cylinders are enclosed by separate meshes (overset grid approach), all within a vortex-transport grid to enable the convection of vortices with low numerical dissipation. This vortex-transport grid itself is encompassed by a background grid that represents the farfield. The computational setup is characterized by various parameters, which are listed in Table 1. The preliminary computations are performed for a free-stream velocity $\mathrm{U}_\infty = 50\,\mathrm{m/s}$ and a cylinder rotational speed $\omega = 6\,\mathrm{Hz}$. The outer diameter of the cylinder, wall thickness, and gap between the airfoil and RSC are set to $0.06c$, $0.01c$, and $0.05c$, where c denotes the chord length of the airfoil. These specific values were explored experimentally in a preliminary test campaign in a small wind tunnel facility at the DLR Institute of Aeroelasticity. For instance, it was found that the airfoil-RSC gap value shall be minimized, so as to increase the gust amplitude. Notably, the gust generator's distance to the downstream observer point, d_i, is explored (i.e., the location at which the model wing, or measurement probe, is placed).

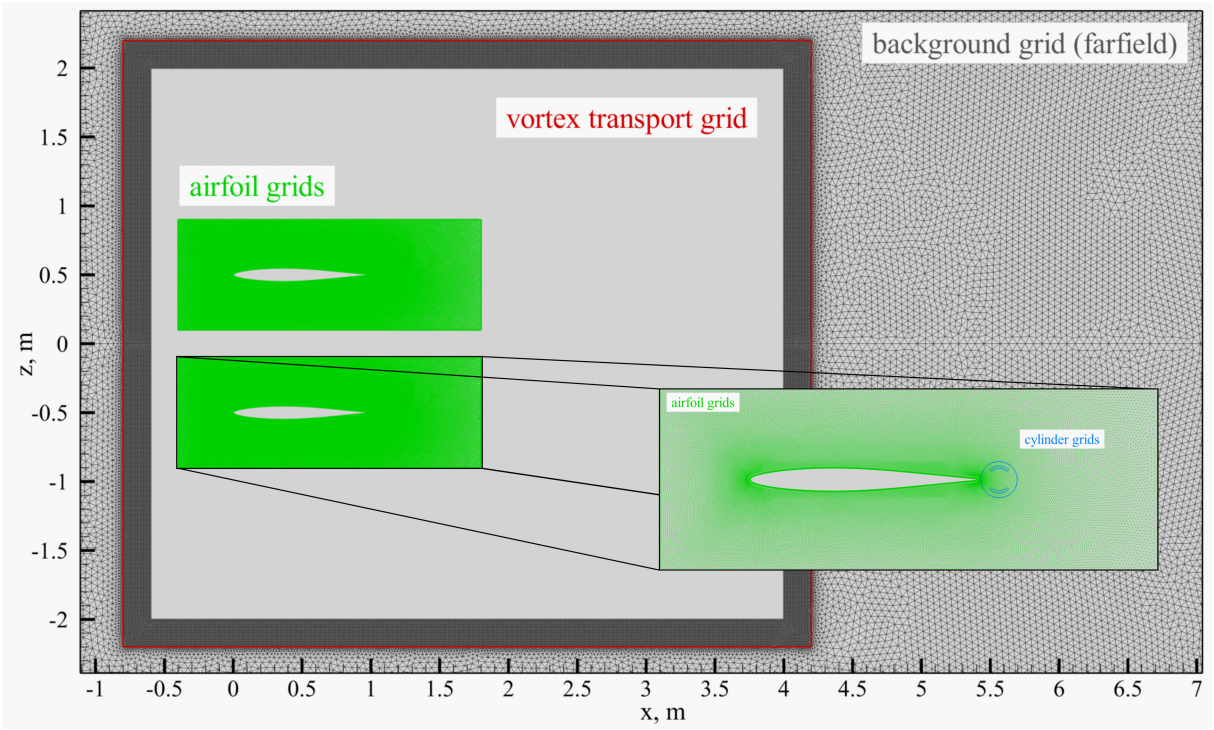

Figure 2: Setup of the computational (overset) grids used for the preliminary 2D URANS CFD studies.

Table 1: Setup parameters of the CFD computations.

U_∞ [m/s]	ω [Hz]	D_{RSC}	t_{RSC}	e_{RSC}	d_i
50	6	0.06c	0.01c	0.05c	0.8-1.2c

Upon initial numerical computations, it was decided to use a custom (symmetric) airfoil for the fixed wings ahead of the cylinders, which is designed using a combination of the Eppler's method and XFOIL [23, 24] with particular emphasis put on a high thickness to achieve higher structural stiffness and strength of the wing. However, to avoid flow separation due to the increased thickness, the upper and lower airfoil contours are designed to have a very low adverse pressure gradient for the sake of a smooth pressure recovery. Laminar separation bubbles should not appear down to a Reynolds number of 5×10^5 (assuming a turbulence level in the wind tunnel of $0.16\,\%$, upon which the critical amplification factor $N_{crit} = 7$), which is expected as the lower limit for the operation in the wind tunnel. The airfoil has a maximum thickness of $16.6\,\%$ at a chordwise position $x/c = 23.9\,\%$, as shown in Fig. 3, alongside its pressure distribution for a Reynolds number of 5×10^5.

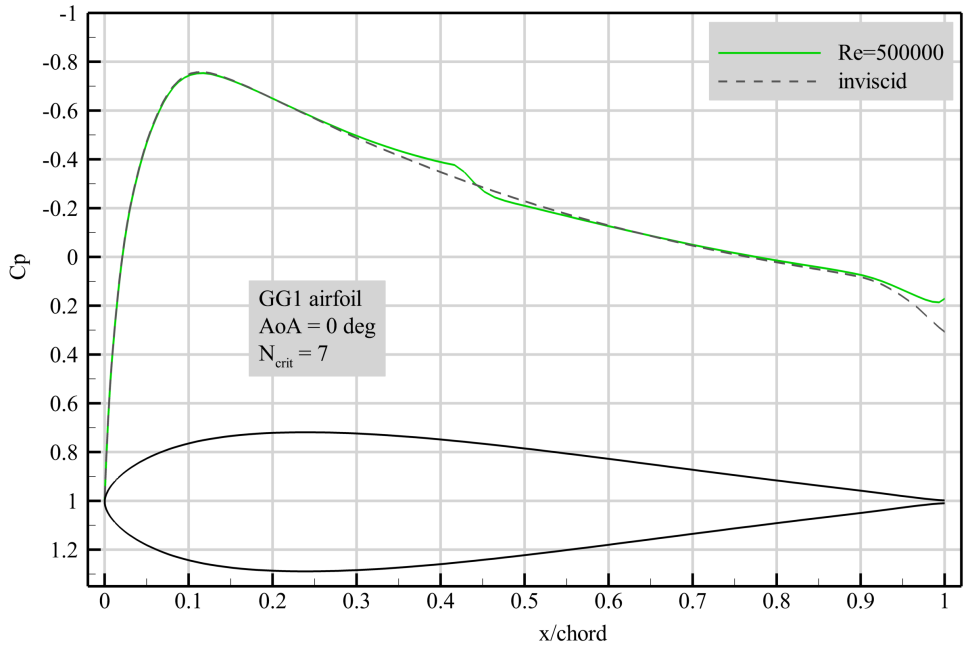

Figure 3: GG1 airfoil designed for the fixed wings ahead of the rotating cylinder, showing its pressure distribution at an angle of attack $\alpha = 0\,^\circ$ and Reynolds number $Re = 5 \times 10^5$ as predicted by XFOIL.

3.2 Computational Results

For the above setup and parameters, the aerodynamic forces and wake flow characteristics of the airfoil-RSC gust generator are computed, to serve as basis for the structural modeling and guideline for test parameters in the subsequent experimental characterization. As can be seen from Fig. 4, the fixed (symmetric) airfoil experiences periodic loads of significant amplitude due to the disturbances from the rotating cylinders. More specifically, the time-varying lift coefficient observed for the airfoil exhibits a maximum lift coefficient C_L of 0.5, which is used as input for the sizing of the RSC structure. Similar observations are also seen for the RSC itself, which experiences a rotation-induced lift of up to $\mathrm{F_{mag}} = 200\,\mathrm{N/m}$ that varies periodically with time.

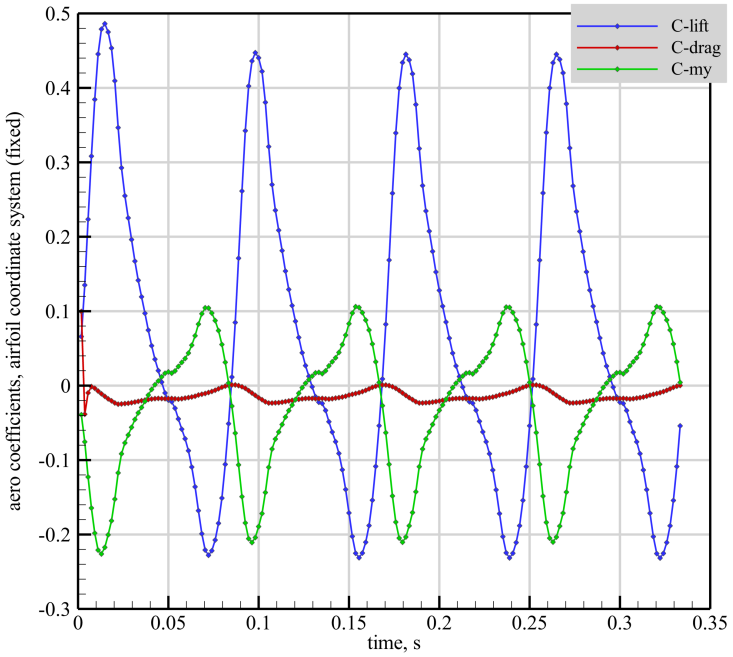

Figure 4: Aerodynamic loads generated by the stationary airfoil.

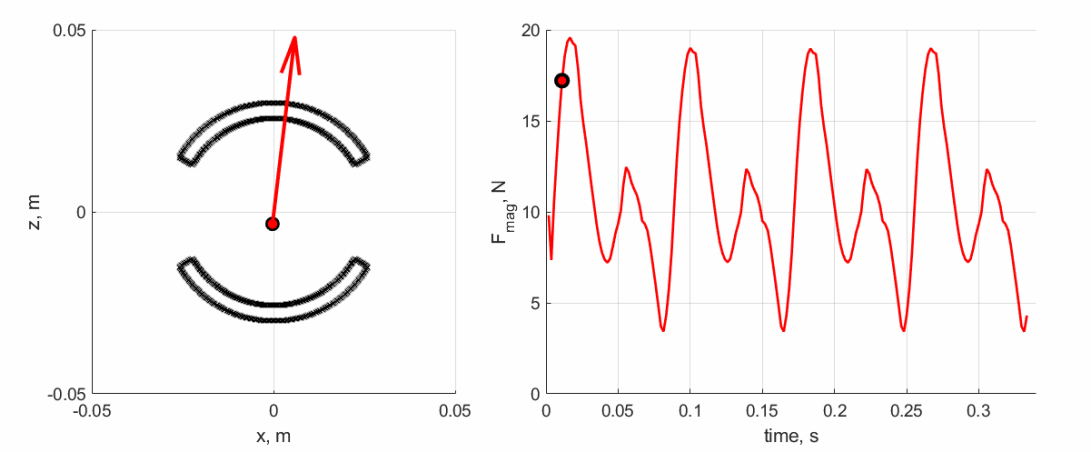

Figure 5: Aerodynamic loads generated by the rotating slotted cylinder.

Regarding the wake flow characteristics induced by the airfoil-RSC gust generator, Fig. 6 depicts the wakes generated behind the cylinder with its slot being parallel and perpendicular to the incoming flow. Additionally, a time history of the gust-flow angle is shown, according to which the gust's amplitude becomes smaller at an observer location that is further downstream (cf. p_1 and p_2).

Upon the above computational results, the structural models of the airfoil and the RSC are examined next in terms of their response towards predefined load cases.

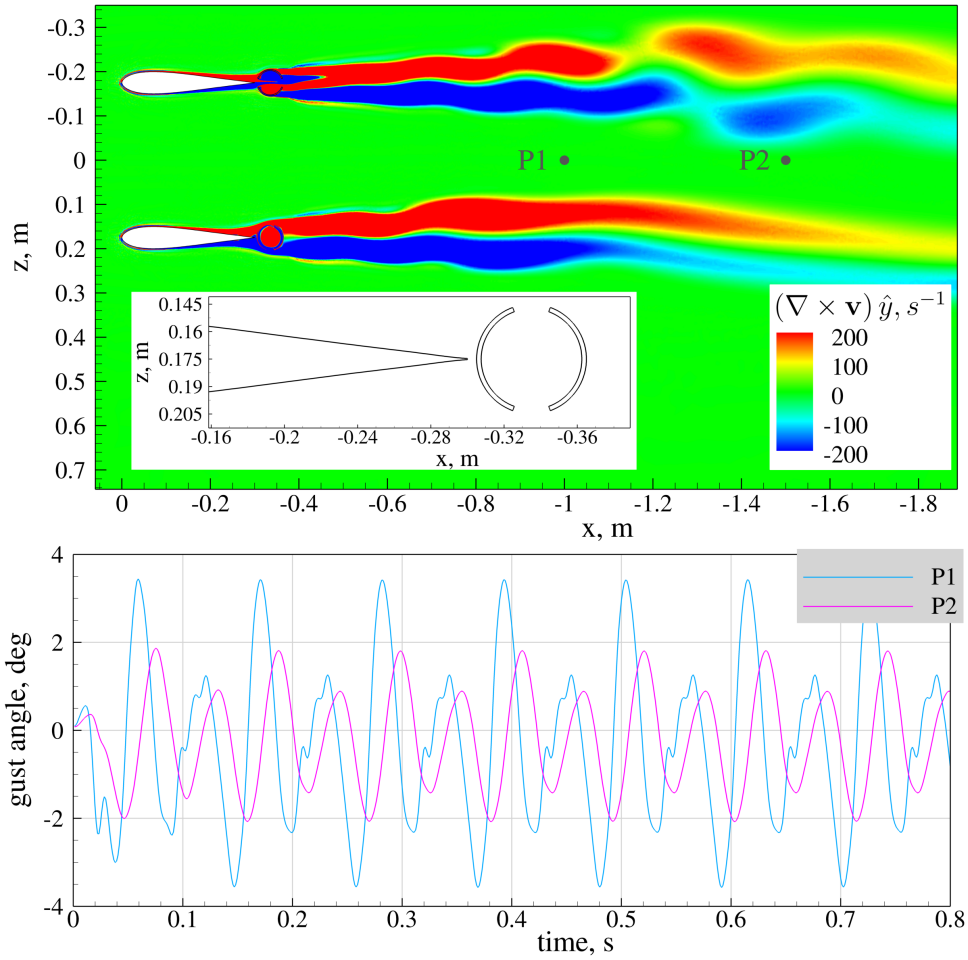

Figure 6: Wake flow and gust angle induced by the gust generator consisting of two airfoils followed by downstream rotating slotted cylinders.

4 STRUCTURAL DESIGN

This section concerns the structural design of the airfoil-RSC gust generator, for which first structural models of both the stationary airfoil and the slotted cylinder are generated before they are analyzed regarding specifically chosen load cases.

4.1 Structural Model

The structural models of both gust-generator components (i.e., airfoil and cylinder) are developed using the DLR in-house parametric modeling environment *ModGen* [25], in which Nastran finite element (FE) representations are generated that are then analyzed with respect to their structural responses upon specific exerted loads.
First, the airfoil's FE model is looked upon - see Fig. 7: This model consists of load carrying wing skins extending from leading to trailing edge that are supported by shear webs and ribs - all of which are discretized as shell elements. The aerodynamic forces exerted on the airfoil are calculated using a doublet lattice model (DLM), which - due to the airfoil's 2D-symmetry and no-twist characteristics - does not require corrections to the local angle of attack. A set of specific nodes is configured across the ribs that allows the coupling of the structural and aerodynamic models. For each rib, all corresponding nodes merge at one centralized point at the airfoil's quarter-chord position. Linking these centralized nodes across the wingspan represents the load reference axis, against which structural deformations and twist responses are

compared. Notably, non-structural masses may be included in specific points of the model to somewhat account for the addition of actuators and other non-negligible weights.

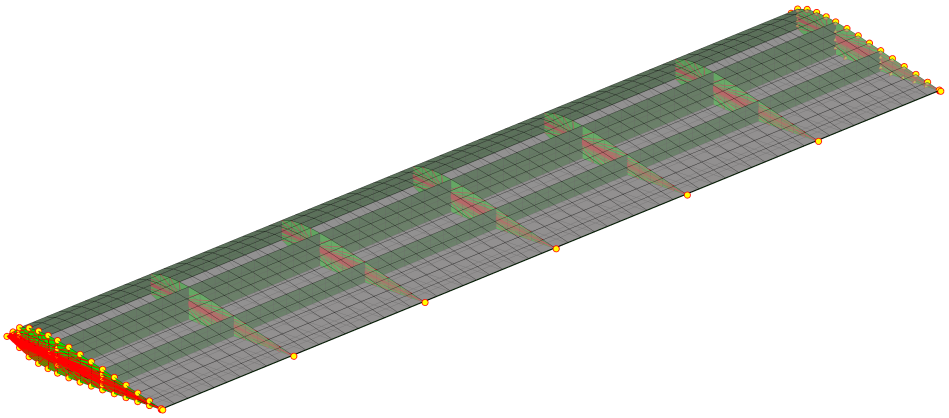

Figure 7: Finite element model of the stationary airfoil, within the gust generator.

The structural model of the slotted cylinders is based upon a similar design approach (cf. Fig. 8), in which the cylinder walls can be seen as the wing's skin (i.e., represented by shell elements). Here too, the ribs act as a coupling agent between the two cylinder walls. The coupling between the structural and aerodynamic models (DLM) is analogue to the approach discussed above. For further details on the modeling approach of the structural models, the reader is referred to the dissertation on this matter [26].

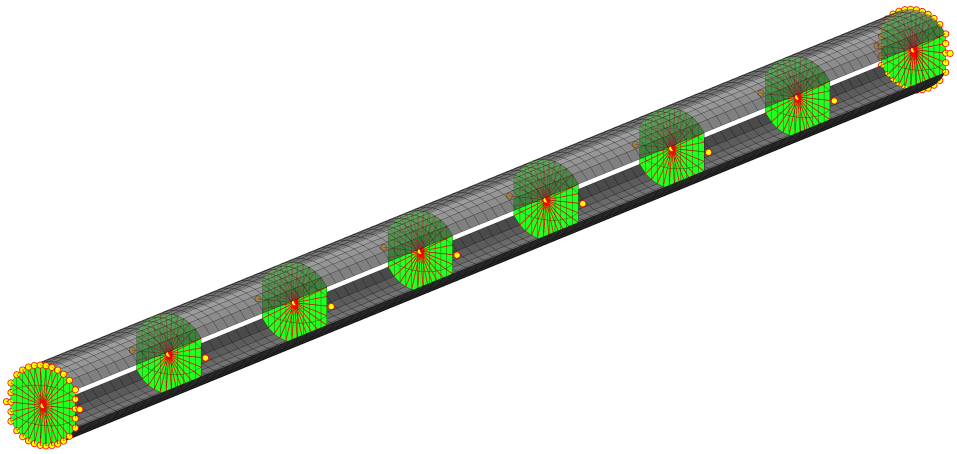

Figure 8: Finite element model of the slotted cylinder, within the gust generator.

4.2 Structural Results

Based upon the structural models representing the airfoil and RSC, load and stress analyses are performed for specifically chosen test cases to not only clear the gust generator for operation in the DNW-NWB tunnel, but also to characterize its structural properties (e.g., eigenfrequencies) that could ever be excited by the inflow or self-induced unsteady motion. To prevent the gust generator's eigenfrequencies to fall within the range of gust excitation, both the airfoil and RSC components are made out of *Dialead K63716* ultra-high modulus fiber, with an E-modulus of 639 GPa.

The structural response of the gust-generator airfoil is evaluated with respect to one critical load case, LC_{A1} (see Table 2). Here, it is worth noting that the numerically predicted lift coefficient ($C_L = 0.5$, cf. Fig. 4) is doubled (i.e., $C_L = 1.0$) to incorporate an additional safety factor of 2.

Table 2: Stationary airfoil - load case.

Load Case	U_∞ [m/s]	ρ [kg/m³]	ω [Hz]	C_L
LC_{A1}	50	1.225	4.5	1.0

For this particular load case, the ply orientation in the wing skin (i.e., the so-called wing skin lay-up) is specifically chosen to maximize the wing's stiffness, whilst maintaining a sufficient structural integrity regarding the required safety factor. This optimized wing skin layup is shown in Fig. 9; As can be seen, both upper and lower wing skins consist of seven ply layers of varying fiber angles.

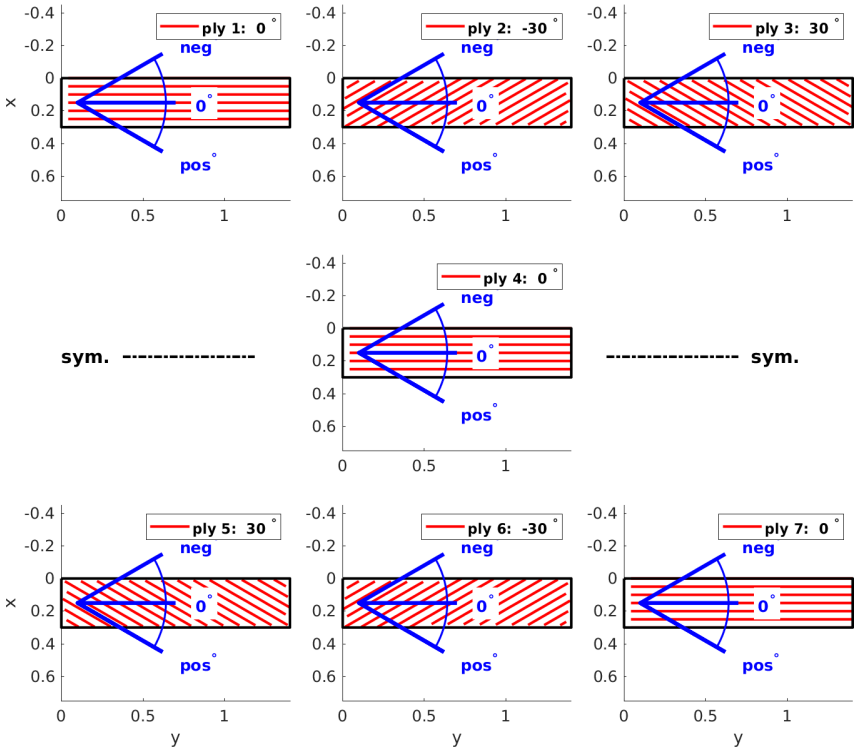

Figure 9: Wing skin layup of the stationary airfoil's suction and pressure side.

Upon this particular fiber layup, a resulting failure index, f_i, can be calculated

$$f_i = \frac{\epsilon_{act}}{\epsilon_{max}} \tag{1}$$

which constitutes the ratio of the actual and the allowable strain - the latter being $0.44\,\%$ and $0.2\,\%$ for tensile and compressive failure, respectively. This index is thus representative of fiber failure for a value of $f_i = 1$. The failure index for each ply layer is shown in Fig. 10, thereby indicating possible safety factors with respect to a failure in fiber direction under the defined load case (LC_{A1}). The results reveal that none of the failure indices exceeds roughly $3\,\%$, thus corresponding to a large safety margin of approximately 30.

Aside from this, the airfoil's deflection across the span under this specific loading is examined. It is found that the airfoil bends less than $0.3\,\mathrm{mm}$ at its most critical location, namely its mid-span. Finally, the first eigenfrequency (i.e., the first bending mode) occurs at $113\,\mathrm{Hz}$ (cf. Fig. 11), which is significantly higher than the targeted gust-flow frequencies and, in turn, an undesired excitation of the airfoil's eigenmodes can thus be neglected.

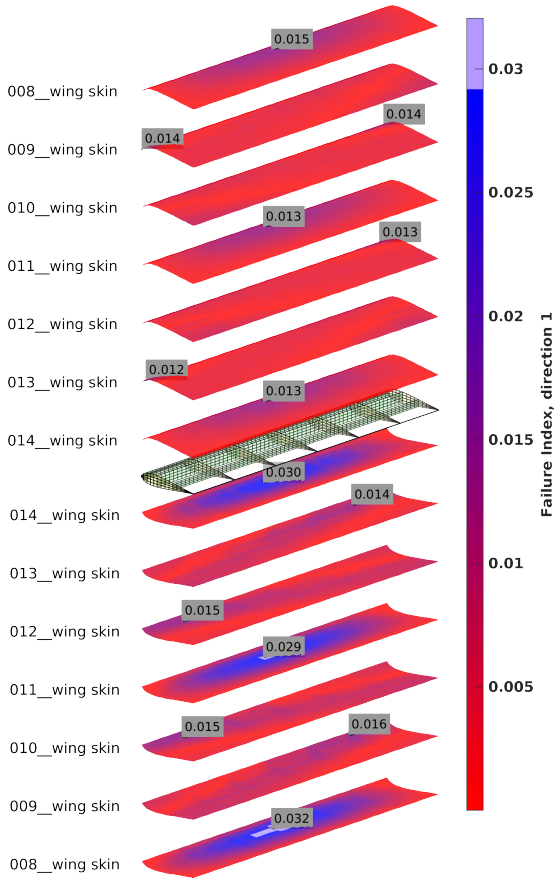

Figure 10: Failure indices in fiber direction under the critical load case (LC_{A1}).

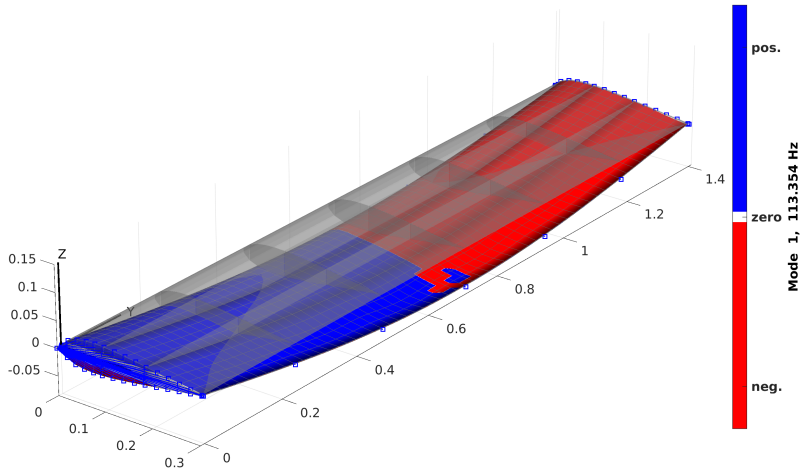

Figure 11: Illustration of the stationary airfoil's first eigenmode (here corresponding to its first bending mode).

In contrast to the stationary airfoil, the structural analysis of the rotating slotted cylinders is conducted for three specific load cases (cf. Table 3), owing to the possibility of the aerodynamic forces acting in different angles (i.e., $\beta = 0°, 45°, 90°$) with respect to the cylinder's slit - see Figs. 12 and 13. These aerodynamic forces acting upon the cylinder are based on the CFD results obtained previously (cf. Fig. 5), according to which the cylinder exerts a maximum load of $200\,\mathrm{N/m}$ for an inflow wind speed $\mathrm{U}_\infty = 50\,\mathrm{m/s}$ and the RSC rotating at a speed $\omega = 4.5\,\mathrm{Hz}$ - see Table 3.

Table 3: Rotating slotted cylinder - load cases.

Load Case	U_∞ [m/s]	ρ [kg/m³]	ω [Hz]	β [°]
LC_{RSC1}	50	1.225	4.5	0
LC_{RSC2}	50	1.225	4.5	45
LC_{RSC3}	50	1.225	4.5	90

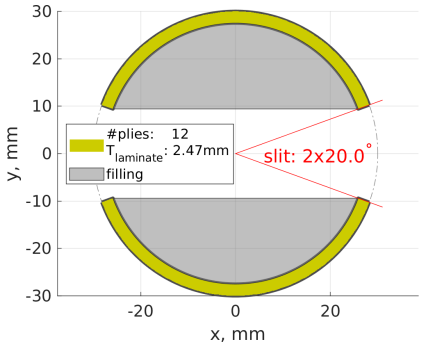

Figure 12: Cross-sectional view of the rotating slotted cylinder (RSC), depicting the slot angle and optional foam fillings (gray).

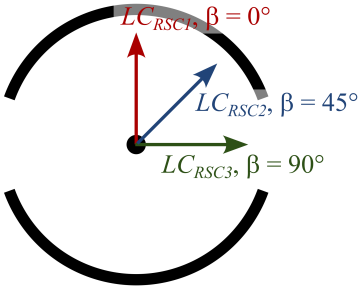

Figure 13: Sketch of the RSC cross-section, illustrating the force direction in each of the three load cases ($LC_{RSC1} - LC_{RSC3}$).

Analogue to the stationary airfoil, the optimized stacking sequence of the upper and lower RSC shell (i.e., the ply book) is shown in Fig. 14, whose resulting failure indices for the more critical load cases LC_{RSC1} and LC_{RSC2} are depicted in Figs. 15 and 16, respectively. As can be seen, the maximum failure index is found to be roughly $4\,\%$, thus constituting a large safety margin of 24 with respect to fiber failure. Besides, the calculated deflection at the RSC's mid-span is considered negligible, due to its rather small value for all load cases (i.e., $<0.7\,\mathrm{mm}$), similar to the airfoil's results. The corresponding first eigenmode of the RSC is characterized at a rather high eigenfrequency of $128.5\,\mathrm{Hz}$), as can be seen from Fig. 17.

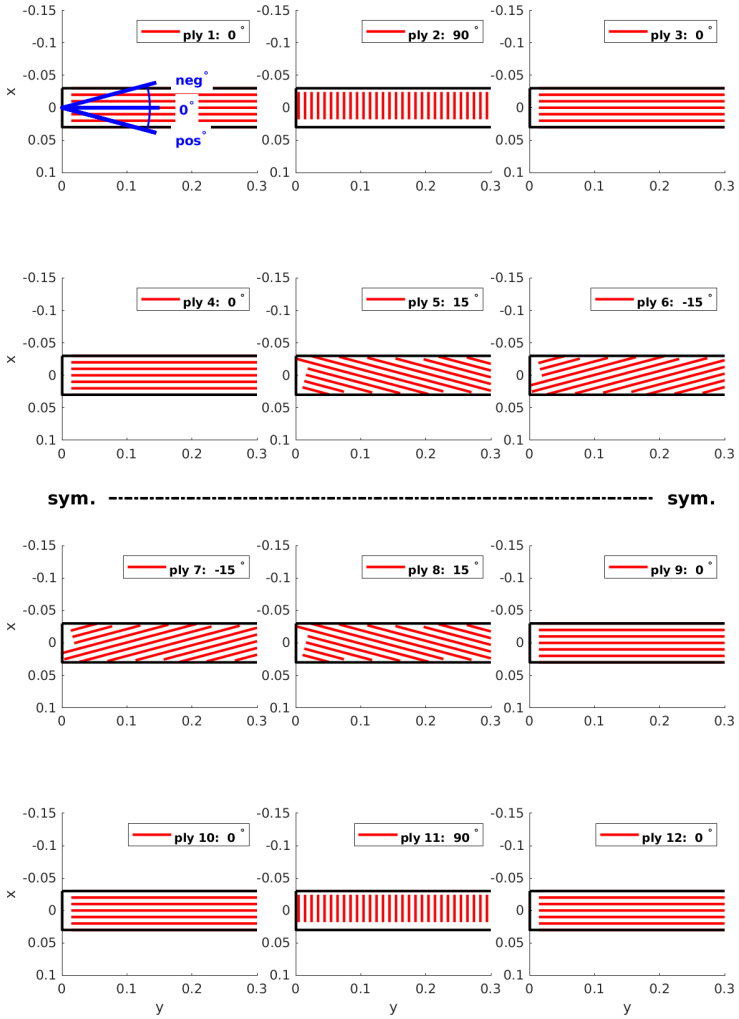

Figure 14: Wing skin layup of the RSC's upper and lower shells.

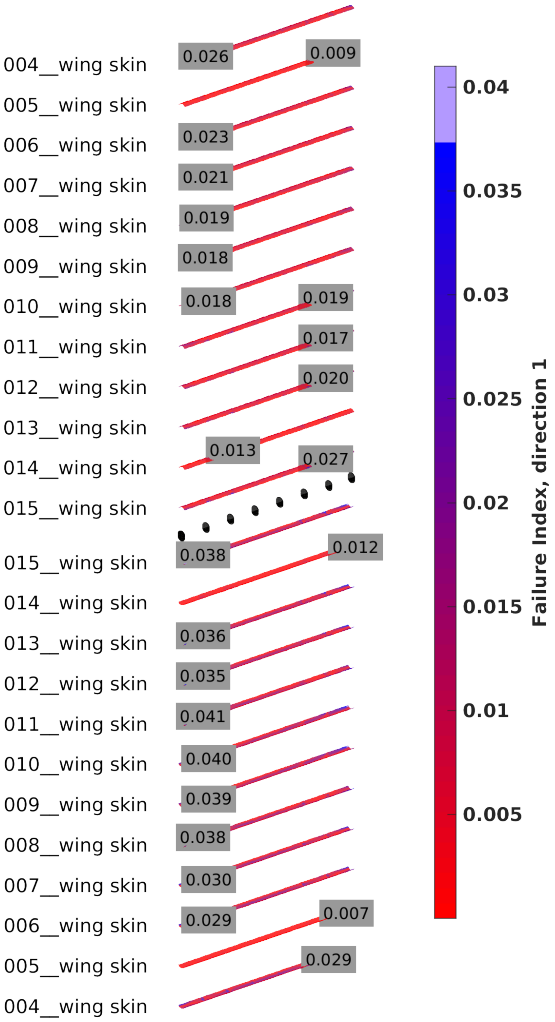

Figure 15: Failure indices in fiber direction under the $\beta = 0°$ load case (LC_{RSC1}).

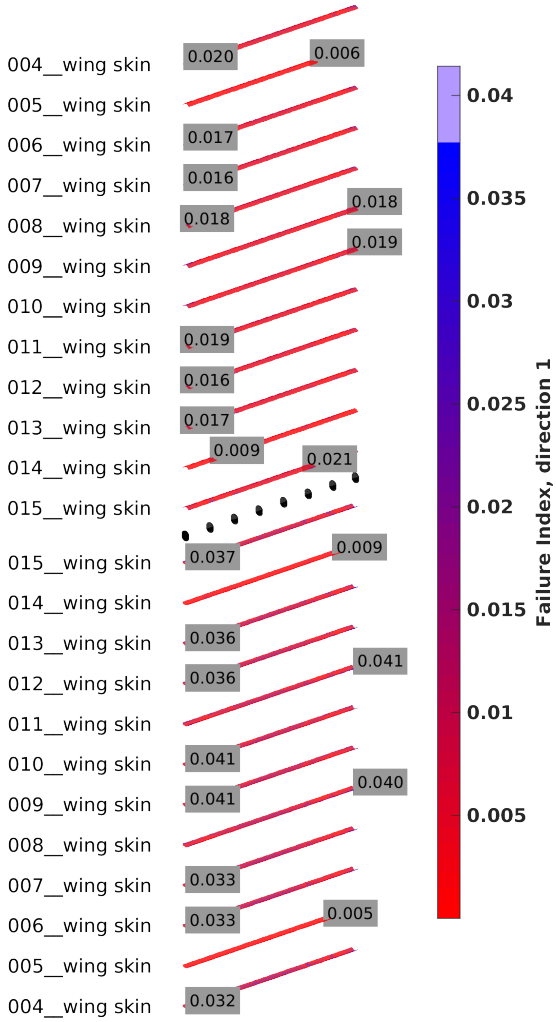

Figure 16: Failure indices in fiber direction under the $\beta = 45°$ load case (LC_{RSC2}).

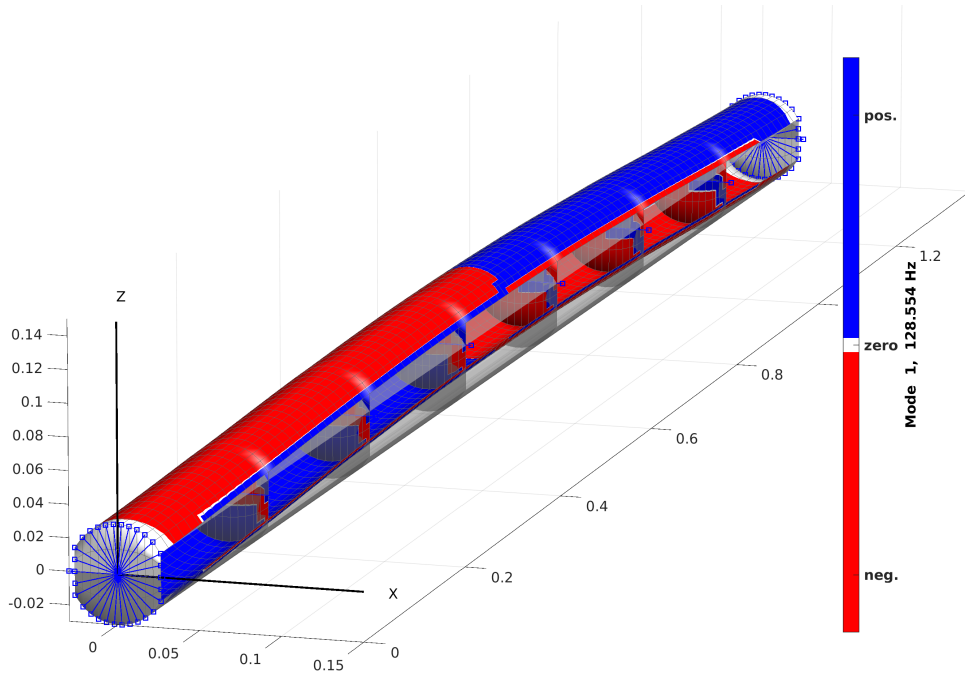

Figure 17: Illustration of the RSC's first eigenmode (here corresponding to its first bending mode).

5 EXPERIMENTAL CHARACTERIZATION

In this section the experimental results characterizing the gust generator's wake flow is looked upon, which are obtained during the wind tunnel test campaign.

5.1 Experimental Setup & Means

The experimental test campaign is conducted in the DNW-NWB, a low-speed wind tunnel of Göttinger type (i.e., closed-loop) - see Fig. 18 - that is located on the DLR site in Braunschweig and operated by the German-Dutch Wind Tunnels (DNW) organization. This tunnel features a closed-vein test section of dimensions $3.25\,\mathrm{m}$ (W) $\times$ $2.8\,\mathrm{m}$ (H) $\times$ $8.0\,\mathrm{m}$ (L), whose inflow can reach mean speeds of $\mathrm{U}_\infty = 0 - 90\,\mathrm{m/s}$ at low turbulence intensities of $Ti < 0.06\,\%$. As indicated in Fig. 18, the gust generator is installed in the test-section area, upstream of a 360° rotational turntable, on which a test model (e.g., an aircraft wing) can be mounted.

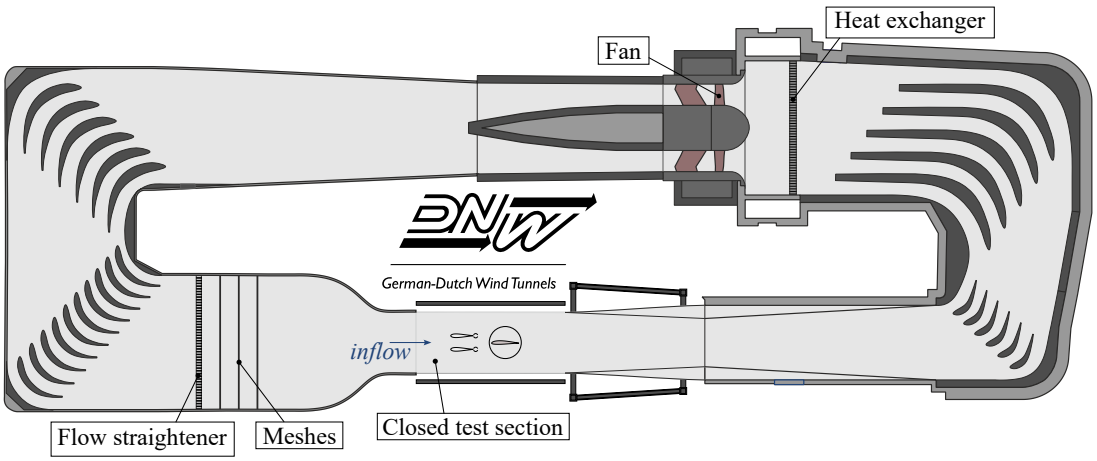

Figure 18: Schematic of low-speed wind tunnel DNW-NWB.

In the present test campaign, however, such a test model is replaced by a two-dimensional traverse that allows for a 5-hole probe to be moved within the tunnel vein's width-height plane - see Fig. 19. The device is fixed at a certain location downstream of the gust generator, whose x-coordinate can be adjusted using an aluminum pipe. The measurement probe used is an unsteady, fast-response 5-hole pressure probe (brand *Vectoflow*) that is capable of capturing flow angles with an accuracy of $\pm 1^\circ$ for an angular range of $\pm 60^\circ$ at a sampling frequency of up to $f_s = 5\,\mathrm{kHz}$. The measurement probe is encompassed by a 3D-printed airfoil-shaped cover that simultaneously fixes the probe at the aluminum pipe's tip and provides an aerodynamically favorable exterior to minimize drag-induced vibrations.

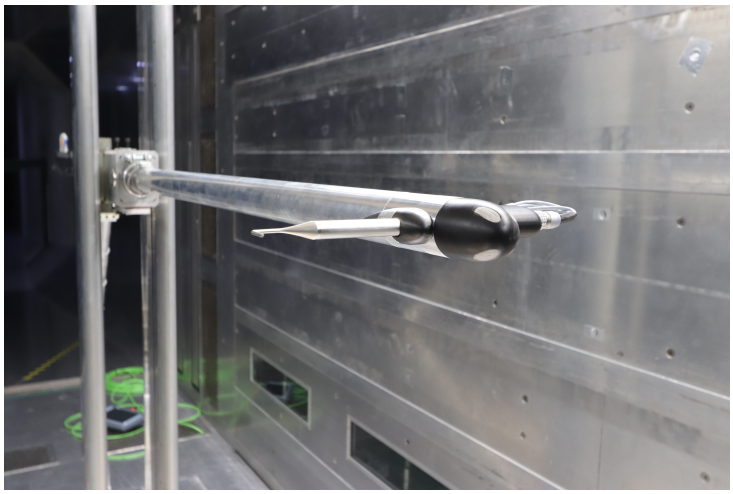

Figure 19: Image of the unsteady, fast-response 5-hole measurement probe mounted on the 2D traverse, downstream of the gust generator.

The airfoil-RSC gust generator is installed on grooved panels on both tunnel floor and ceiling, thereby spanning the entire vein height - see Fig. 20. The panels allow for a variation in the gust generator's streamwise (x) position, as well as the spacing s between the two airfoil-RSC elements. Besides, a horizontal steel wire spans the wind tunnel, stiffening the gust generator by being fixated at its mid-span. Here, each gust-generator unit (i.e., airfoil + RSC) is divided into a bottom and top half, connected via a coupling element in its mid-span (e.g., a metal bellows coupling to link the two RSC halves that is chosen to compensate for potential installation misalignment). Notably, in future experiments, two additional gust-generator units are manufactured, thus guaranteeing a more coherent wake gust across the full wind tunnel width.

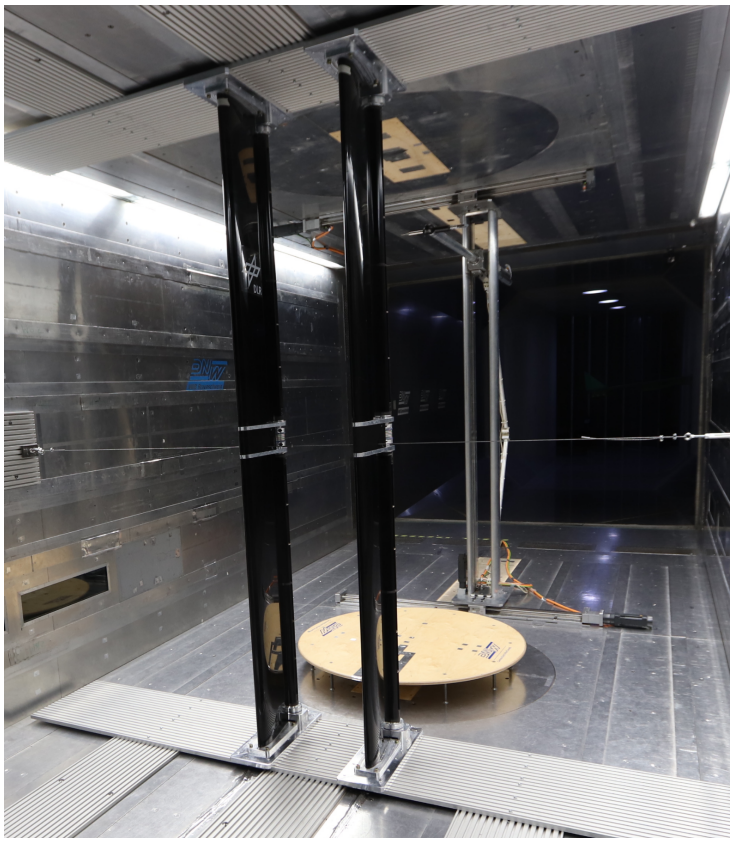

Figure 20: Image of the unsteady, fast-response 5-hole measurement probe mounted on the 2D traverse, downstream of the gust generator.

What concerns the experimental matrix, the 5-hole probe is traversed across various locations in all three dimensions, roughly spanning $1\,\mathrm{m}$ in y and $1.5\,\mathrm{m}$ in z, which is done for three selected x coordinates (i.e., approximately $x = 0.5, 1.0, 1.5\,\mathrm{m}$ downstream of the gust generator). Aside from this, measurements are obtained at different inflow wind speeds (i.e., $\mathrm{U}_\infty = 30, 40, 50\,\mathrm{m/s}$). Finally, continuous as well as discrete gusts are generated, the latter of which being looked at for one condition.

5.2 Experimental Results

First, unfiltered results for the horizontal gust angle (α_g) and the vertical yaw angle (γ) are depicted in Fig. 21, characterizing the wake flow at a downstream location $x = 1.0\,\mathrm{m}$ for an inflow speed $\mathrm{U}_\infty = 30\,\mathrm{m/s}$. As can be seen, the gust generator induces a wake flow that periodically varies in time for the horizontal gust angle (α_g) - as desired. In contrast, the flow exhibits little variation with respect to its vertical deflection, as revealed by the small changes in the γ values. At this stage, the measured signal exhibits some noise, albeit the signal-to-noise ratio being acceptable enough. To isolate the periodic gust flow more explicitly, an infinite impulse response (IIR) filter is applied to the time-series data - cf. Fig. 22.

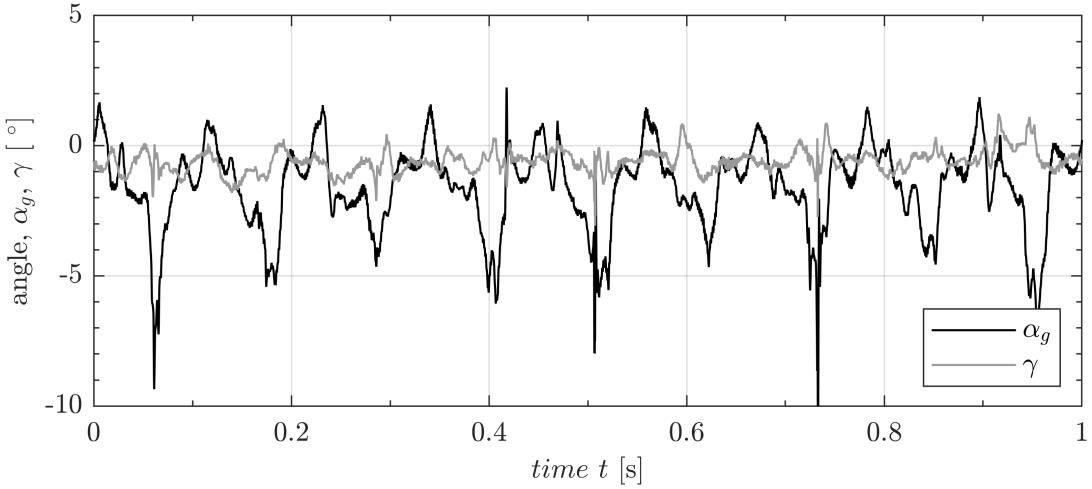

Figure 21: Gust and vertical angles generated by the gust generator rotating at $\omega = 4.5\,\mathrm{Hz}$, as obtained in the wake at $x = 1.0\,\mathrm{m}$ and $\mathrm{U}_\infty = 30\,\mathrm{m/s}$.

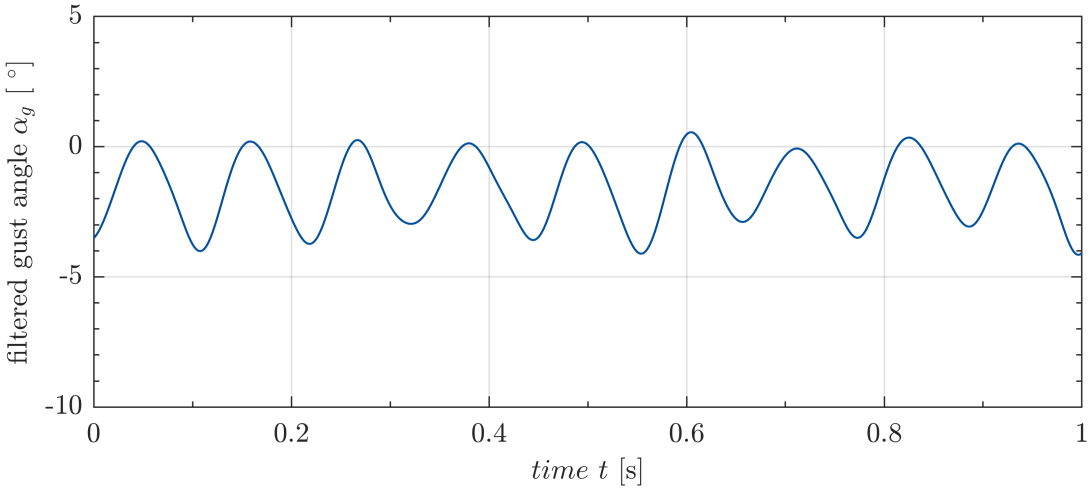

Figure 22: IIR-filtered gust angle induced by the gust generator rotating at $\omega = 4.5\,\mathrm{Hz}$, as obtained in the wake at $x = 1.0\,\mathrm{m}$ and $\mathrm{U}_\infty = 30\,\mathrm{m/s}$.

Upon this IIR-filtered gust angle, it can be seen that a wake gust of 5° amplitude is generated under these inflow conditions. Besides, by simply counting the number of peaks over this $T = 1\,\mathrm{s}$ interval (here 9 peaks), the set RSC rotational speed of $\omega = 4.5\,\mathrm{Hz}$ corresponds to a $\omega_g = 9\,\mathrm{Hz}$, as expected. This relationship is further seen when examining the spectral content of this gust signal, which is shown in Fig. 23. The PSD results reveal that the gust angle α_g exhibits the highest spectral energy content at $\omega_g = 9\,\mathrm{Hz}$ and its subsequent harmonics (i.e., $18, 27, 36\,\mathrm{Hz}$, etc.).

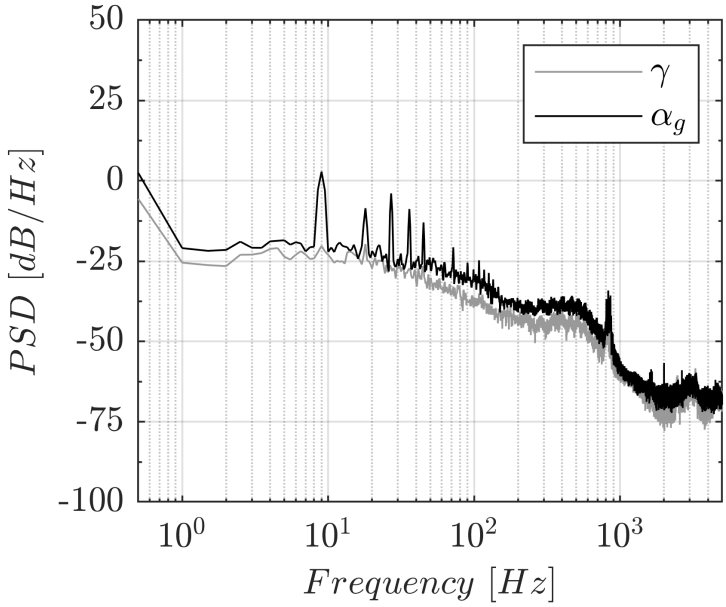

Figure 23: Spectral analysis of the gust-angle signals when converted using the common *pWelch* method for the gust generator rotating at $\omega = 4.5\,\mathrm{Hz}$, as obtained in the wake at $x = 1.0\,\mathrm{m}$ and $\mathrm{U}_\infty = 30\,\mathrm{m/s}$.

In comparison to the gust flow obtained behind the RSC, the flow behind the generator's coupling element (i.e., at mid-span) still exhibits the periodic angular variation, albeit at lower amplitudes - cf. Fig. 24. While the coupler induces a weaker gust flow in the center of the test vein, the wake flow becomes more disturbed as the probe is moved away from the *x*-*z* plane, closer towards the downstream location directly behind the rotating cylinders. For the sake of conciseness, these results are however not shown here.

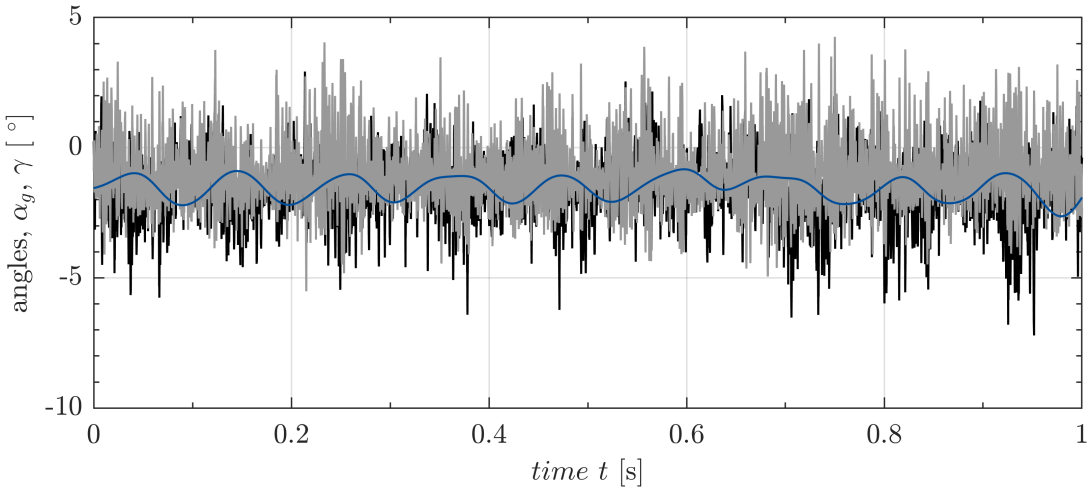

Figure 24: Gust and vertical angles generated by the gust generator rotating at $\omega = 4.5\,\mathrm{Hz}$, as obtained in the wake at mid-span height at $x = 1.0\,\mathrm{m}$ and $\mathrm{U}_\infty = 30\,\mathrm{m/s}$.

Beyond the continuous gusts induced by the constant spin of the generator's cylinders, discrete rotations are also performed whose wake characteristics exhibit discontinuous flow sequences. Figure 25 depicts a time interval comprising $T = 5\,\mathrm{s}$, in which one discrete gust corresponding to a clockwise 180° rotation of the RSC is captured. As can be seen, two distinct peaks emerge due to the discrete rotation of the rotating, slotted cylinders. Notably, these gust peaks constitute a negative (resp. positive) angle depending on the RSC's rotation being clockwise (resp.

counter-clockwise).

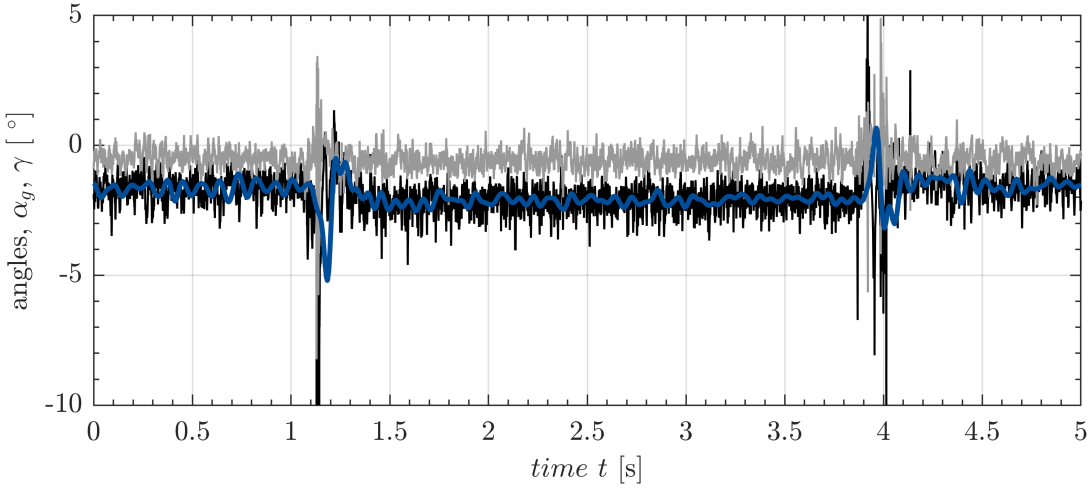

Figure 25: Discrete gust signal generated by the gust generator rotating with a frequency $\omega = 4.5\,\mathrm{Hz}$, when obtained in the wake at $x = 1.5\,\mathrm{m}$ and $\mathrm{U}_\infty = 50\,\mathrm{m/s}$.

Upon the above experimental characterization, the airfoil-RSC gust generator has the capacity of inducing highly periodic gust flow, with sufficiently large angles whether this being for continuous or discrete events. Therefore, the current device is found suitable for exploring the gust response of flexible aircraft structures (e.g., a wing model) and the effectiveness of gust-load alleviation techniques, such as control surfaces that are actively driven by a load-control algorithm.

6 CONCLUSIONS & PERSPECTIVES

The present work described the design of a gust generator for the low-speed wind tunnel DNW-NWB that is based upon stationary airfoils followed by rotating slotted cylinders (RSC). This gust-generator was first conceptualized according to the technical requirements both in terms of flow characteristics as well as the dimension of the wind-tunnel facility. Numerical computations were performed for both the aerodynamic wake flow and structural properties of the device. Various design parameters were evaluated, which shaped the final gust generator that was ultimately manufactured and installed in the tunnel vein. An experimental test campaign to characterize the device's gust-generating capacity was conducted using an unsteady, fast-response 5-hole probe mounted to a two-dimensional traverse system. Results revealed that the airfoil-RSC gust generator produces a periodic horizontal gust flow at various downstream locations, whether this concerns continuous or discrete gust events. While the measurements exhibit sufficiently promising gust-flow characteristics for exploring the aeroelastic gust response by aircraft wings, future work is dedicated to extend the present gust generator (two airfoil-RSC units) to four airfoils with RSCs and to investigate more sophisticated motor controls (e.g., RSCs counter-rotate with/out predefined phase lags).

7 REFERENCES

[1] Dessi, D. and Mastroddi, F. (2008). A nonlinear analysis of stability and gust response of aeroelastic systems. *Journal of Fluids and Structures*, 24(3), 436–445. ISSN 08899746. doi:10.1016/j.jfluidstructs.2007.09.003.

[2] Raveh, D. E. (2007). CFD-Based Models of Aerodynamic Gust Response. *Journal of Aircraft*, 44(3), 888–897. ISSN 0021-8669, 1533-3868. doi:10.2514/1.25498.

[3] Raveh, D. E. (2011). Gust-Response Analysis of Free Elastic Aircraft in the Transonic Flight Regime. *Journal of Aircraft*, 48(4), 1204–1211. ISSN 0021-8669, 1533-3868. doi:10.2514/1.C031224.

[4] Neumann, J. and Mai, H. (2013). Gust response: Simulation of an aeroelastic experiment by a fluid–structure interaction method. *Journal of Fluids and Structures*, 38, 290–302. ISSN 08899746. doi:10.1016/j.jfluidstructs.2012.12.007.

[5] Lancelot, P. M., Sodja, J., Werter, N. P., et al. (2017). Design and testing of a low subsonic wind tunnel gust generator. *Advances in aircraft and spacecraft science*, 4(2), 125–144. doi:10.12989/AAS.2017.4.2.125.

[6] Brion, V., Lepage, A., Amosse, Y., et al. (2015). Generation of vertical gusts in a transonic wind tunnel. *Experiments in Fluids*, 56(7), 145. ISSN 0723-4864, 1432-1114. doi: 10.1007/s00348-015-2016-5.

[7] Saddington, A., Finnis, M., and Knowles, K. (2015). The characterisation of a gust generator for aerodynamic testing. *Proceedings of the Institution of Mechanical Engineers, Part G: Journal of Aerospace Engineering*, 229(7), 1214–1225. ISSN 0954-4100, 2041-3025. doi:10.1177/0954410014548237.

[8] Fonte, F., Riccobene, L., Ricci, S., et al. (2016). Design, Manufacturing and Validation of a Gust Generator for Wind Tunnel Test of a Large Scale Aeroelastic Model. In *30th Congress of the International Council of the Aeronautical Sciences*. Daejeon, Korea, p. 9.

[9] Balatti, D., Haddad Khodaparast, H., Friswell, M. I., et al. (2022). Improving Wind Tunnel "1-cos" Gust Profiles. *Journal of Aircraft*, 59(6), 1514–1528. ISSN 1533-3868. doi: 10.2514/1.C036772.

[10] Wu, Z., Zhang, T., Gao, Y., et al. (2024). Development of a Novel Small-Scale Gust Generator Research Facility. *Aerospace*, 11(1), 95. ISSN 2226-4310. doi: 10.3390/aerospace11010095.

[11] Fernandez, F., Cleaver, D., and Gursul, I. (2020). Unsteady aerodynamics of a wing in a novel small-amplitude transverse gust generator.pdf. *Experiments in Fluids*, 62(9), 20. doi:https://doi.org/10.1007/s00348-020-03100-8.

[12] Olson, D. A., Naguib, A. M., and Koochesfahani, M. M. (2021). Development of a Low-Turbulence Transverse-Gust Generator in a Wind Tunnel. *AIAA Journal*, 59(5), 1575–1584. ISSN 0001-1452, 1533-385X. doi:10.2514/1.J059962.

[13] Wood, J., Breuer, M., and Neumann, T. (2022). A novel approach for artificially generating horizontal wind gusts based on a movable plate: The Paddle. *Journal of Wind Engineering and Industrial Aerodynamics*, 230, 105170. ISSN 01676105. doi:10.1016/j.jweia.2022.105170.

[14] Vernon, L. (1993). In-flight Investigation of a Rotating Cylinder-Based Structural Excitation System for Flutter Testing. Technical Memorandum NASA-TM-4512, NASA, La Jolla,CA,U.S.A.

[15] Cizmas, P. G. A., Tang, D., and Dowell, E. H. (1996). Flow about a slotted cylinder-airfoil combination in a wind tunnel. *Journal of Aircraft*, 33(4), 716–721. ISSN 0021-8669, 1533-3868. doi:10.2514/3.47006.

[16] Tang, D. M., Cizmas, P. G. A., and Dowell, E. H. (1996). Experiments and analysis for a gust generator in a wind tunnel. *Journal of Aircraft*, 33(1), 139–148. ISSN 0021-8669, 1533-3868. doi:10.2514/3.46914.

[17] Krüger, W. R., Mai, H., Kier, T. M., et al. (2024). Assessment of Active Load Control Approaches for Transport Aircraft - Simulation and Wind Tunnel Test. In *International Forum on Aeroelasticity and Structural Dynamics, IFASD 2024*. Den Haag, Netherlands.

[18] Dillinger, J., Mai, H., Krüger, W. R., et al. (2024). Design, manufacturing and identification of an actively controlled flexible wing for subsonic wind tunnel testing. In *International Forum on Aeroelasticity and Structural Dynamics, IFASD 2024*. Den Haag, Netherlands.

[19] Stalla, F., Kier, T. M., Looye, G., et al. (2024). Wind Tunnel Testing Active Gust Load Alleviation of a Flexible Wing. In *International Forum on Aeroelasticity and Structural Dynamics, IFASD 2024*. Den Haag, Netherlands.

[20] Neunaber, I. and Braud, C. (2020). First characterization of a new perturbation system for gust generation: the chopper. *Wind Energy Science*, 5(2), 759–773. ISSN 2366-7451. doi:10.5194/wes-5-759-2020.

[21] Roadman, J. and Mohseni, K. (2009). Gust Characterization and Generation for Wind Tunnel Testing of Micro Aerial Vehicles. In *47th AIAA Aerospace Sciences Meeting including The New Horizons Forum and Aerospace Exposition*. Orlando, Florida: American Institute of Aeronautics and Astronautics. ISBN 978-1-60086-973-0. doi:10.2514/6.2009-1290.

[22] (2023). Easy Access Rules for Large Aeroplanes (CS-25) (Amendment 24).

[23] Eppler, R. (1990). *Airfoil Design and Data*. Springer-Verlag Berlin Heidelberg.

[24] Drela, M. (1989). *XFOIL: An Analysis and Design System for Low Reynolds Number Airfoils*. Berlin, Heidelberg: Springer Berlin Heidelberg, pp. 1–12.

[25] Klimmek, T. (2009). Parameterization of topology and geometry for the multidisciplinary optimization of wing structures. In *Proceedings "CEAS 2009"*. Manchester, UK.

[26] Dillinger, J. (2014). *Static Aeroelastic Optimization of Composite Wings with Variable Stiffness Laminates*. PhD Dissertation, TU Delft, Delft, Netherlands.

ACKNOWLEDGMENTS

The authors would like to express their sincerest gratitude to the technical staff of the Institute of Aeroelasticity at the DLR, namely Mr. T. Büte, Mr. H. Böhlken, Mr. H. Ernst, Mr. M. Löhr, without whom the design and manufacturing of the discussed gust-generator device would not have been feasible. Furthermore, a special thanks goes to Ms. G. Schwetje, who conducted an extensive parametric test campaign at our small-scale wind tunnel facility to gather preliminary experimental results during the conceptual design phase. Finally, the authors would like to thank all colleagues contributing to the completion of this test campaign and thus the overall project,

whether the teams from the DLR - Institute of System Dynamics and Control (Mr. F. Stalla, Mr. T. Kier, Mr. G. Looye) or from the DNW-NWB wind tunnel (Mr. T. Löser et al.). The success of this research project is therefore to a large extent due to their expertise and collective efforts, as much as those of the present authors.

COPYRIGHT STATEMENT

The authors confirm that they, and/or their company or organisation, hold copyright on all of the original material included in this paper. The authors also confirm that they have obtained permission from the copyright holder of any third-party material included in this paper to publish it as part of their paper. The authors confirm that they give permission, or have obtained permission from the copyright holder of this paper, for the publication and public distribution of this paper as part of the IFASD 2024 proceedings or as individual off-prints from the proceedings.